Polyhedron 225 (2022) 116046

Contents lists available at ScienceDirect

Polyhedron

journal homepage: www.elsevier.com/locate/poly

Palladium complexes bearing calixpyrrole ligands with pendant hydrogen bond donors: Synthesis, structural characterization, electrochemistry and dihydrogen evolution

Logan Trowbridge, Boris Averkiev, Peter E. Sues *

Department of Chemistry, Kansas State University, Manhattan, KS 66503, USA

ARTICLE INFO

Keywords:
Palladium complexes
Calixpyrrole ligands
Synthesis
Electrochemistry
Hydrogen evolution

ABSTRACT

A series of three calixpyrrole ligands (**1a-c**) with pendant nitrogen-based hydrogen bond donors, R, were synthesized and coordinated to palladium to produce metal complexes (**2a-c**), where R = NH_2 (**a**); $NHC(O)CH_3$ (**b**); or $NHC(O)OC(CH_3)_3$ (**c**). The calixpyrrole compounds were generated using a Schiff-base reaction starting with 5,5′-diformyl-2,2′-diphenyldipyrromethane and an aniline precursor. The deprotonated calixpyrrole species were subsequently bound to palladium to generate distorted square planar complexes. The pendant groups were not coordinated to the metal with Pd-N distances of 3.36 to 4.79 Å. The electrochemical properties of the palladium complexes were also explored, and **2a-c** displayed two irreversible oxidations above 0.0 V vs ferrocene/ferrocenium (Fc/Fc^+), as well as two irreversible reductions below −0.70 V vs Fc/Fc^+. Interestingly, the free ligands showed similar electrochemical features, suggesting redox non-innocence. Preliminary reactivity studies indicated the palladium complexes did not activate small molecules, but they did catalyze H_2 evolution in the presence of acid. The onset of catalysis for **2a-c** was approximately 0.4–0.5 V more positive than a glassy carbon electrode, and the active species could undergo 500 scans without significant changes in activity. The catalysts were found to be heterogeneous in nature and adsorbed onto the working electrode.

1. Introduction

Despite efforts to curb global reliance on fossil fuels, the use of such non-renewable energy sources has been steadily growing. Through a 20 year span from 1998 to 2018, worldwide fossil fuel consumption has increased >50 %, and future projections predict that these values will continue to rise [1]. In order to avoid the consequences of increased global temperatures [2,3], a substantial shift towards renewable energy sources is needed. To this end, there has been a surge in interest toward the activation of small molecules (such as N_2, CO_2, CH_3OH, H_2, etc.), which will be an integral part of creating a sustainable energy economy [4–8]. One of the current barriers to implementing these technologies, however, is the transfer of multiple electrons and protons that is required for the activation of these types of molecules. While enzymes, such as hydrogenase or nitrogenase enzymes, can efficiently affect these transformations, synthetic catalysts, which often lack the complexity of enzymes, are commonly much less effective than their biological counterparts [9–13].

One approach for facilitating small molecule activation is the placement of a proton shuttle (an acidic or basic moiety) near the catalytic centre to enable the simultaneous transfer of a proton and electron, or proton-coupled electron transfer (PCET) [14–16]. This is commonly seen in protein active sites where the secondary coordination sphere is used to enable catalysis. A well-studied example that illustrates the importance of PCET is the [Fe-Fe]-hydrogenase, which can generate H_2 very efficiently with turnover frequencies > 10,000 s^{-1} [17–19]. The active site of this enzyme has a cofactor with a crucial bridging azadithiolate ligand that acts as a proton shuttle [5,11,17].

In order to mimic enzyme active sites, a large amount of research on synthetic catalysts has focused on designing ligands that can place proton shuttles near the metal centre [20,21]. Rauchfuss *et al.*, [22] have created diiron complexes bearing a pendant amine (via a bridging azadithiolate ligand) meant to mimic the active sites of [Fe-Fe]-hydrogenases (shown in Fig. 1). These complexes were able to participate in H_2 evolution, while operating at overpotentials > 700 mV [22]. Similarly, Bullock *et al.* have developed a series of monometallic nickel diphosphacycloheptane complexes with pendant amines in an effort to mimic the proton shuttling capabilities of natural hydrogenases (shown

* Corresponding author.
E-mail address: psues@ksu.edu (P.E. Sues).

https://doi.org/10.1016/j.poly.2022.116046
Received 4 June 2022; Accepted 12 July 2022
Available online 18 July 2022

in Fig. 1) [5,23–25]. These species are extremely active catalysts and were found to participate in both H_2 evolution and oxidation [5,23–25]. While the turnover frequencies of some of these complexes have eclipsed 100,000 s^{-1}, the impressive catalytic rate is hindered by overpotentials of 625 mV (in comparison to some hydrogenases, which are thought to have overpotentials < 100 mV) [23]. Lastly, Nocera *et al.* have also demonstrated the utility of proton shuttles in electrocatalysis through the development of "hangman" porphyrins (shown in Fig. 1), chlorins, and corroles, which bear a carboxylic acid moiety overhanging the catalytic centre [26–37]. These species were found to be active for O_2 reduction, CO_2 reduction, and H_2 production. Unlike the previously mentioned catalysts, however, the hangman porphyrins could only facilitate the donation of a proton due to the less amphoteric nature of the carboxylic acid functionality. In addition, another drawback of the Nocera "hangman" systems is the difficult ligand synthesis, which hinders systematic modifications to the ligand architecture.

A class of compounds related to porphyrins are macrocyclic Schiff-base calixpyrroles, which were researched independently by the Love group [38–46], as well as Sessler and co-workers [47,48]. Shown in Fig. 2, the co-facial complexes are analogous to the bimetallic "pacman" porphyrins developed by Collman, and many others [49–63]. In contrast to porphyrins, calixpyrrole ligands are prepared in significantly higher yields utilizing a much more facile synthetic route (a Schiff-base reaction) [42]. Moreover, Love and co-workers have studied the use of cobalt "pacman" calixpyrrole complexes for the four-electron reduction of O_2 [40–42]. While they found that these systems do catalytically reduce oxygen, the active species (a bridged superoxo intermediate) is only generated in small amounts, leading to slow turnover [42]. As noted by Love *et al.*, this issue was likely driven by ineffective protonation of the superoxo intermediate, generating a peroxo species which favoured the two-electron reduction of O_2 to H_2O_2 [42]. As such, incorporating proton shuttles into the secondary coordination sphere of the calixpyrrole ligand framework (in order to facilitate PCET) could help generate more effective catalysts for the activation of small molecules.

In this paper, we present the syntheses of Schiff-base calixpyrrole ligands with pendant functional groups, as well as their characterization. These species are similar to the "hangman" porphyrins developed by Nocera *et al.* [26–37] in that the pendant functional groups provide an avenue for controlling the secondary coordination sphere, while also combining the ease of synthesis seen for the "pacman" calixpyrrole compounds [38–46]. In addition, the first metal complexes bearing these ligands, palladium species, are discussed and the coordination geometry of the ligands is investigated. Lastly, the electrochemical properties of the calixpyrrole systems are explored. With respect to nomenclature, throughout this paper the calixpyrrole ligands (**1**) will be named according to their pendant groups (**a** for amino; **b** for acyl; **c** for *tert*-butoxycarbonyl or Boc), while the palladium complexes will be named according to the bound calixpyrrole ligand (**2a-c** for **1a-c**, respectively).

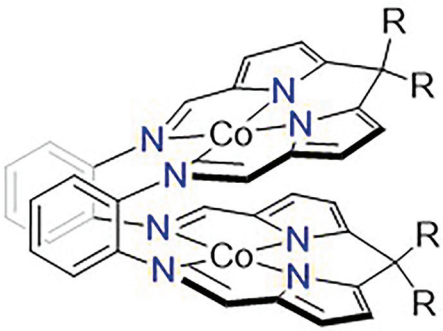

Fig. 2. Example of a binuclear macrocyclic Schiff-base calixpyrrole complex.

2. Results and discussion

2.1. Synthesis and characterization of compounds 1a-c

Compounds **1a-c** were synthesized using an acid catalyzed Schiff-base reaction (Scheme 1). One equivalent of 5,5′-diformyl-2,2′-diphenyldipyrromethane was combined with an appropriate aniline precursor (*ortho*-phenylenediamine for **1a**, *N*-(2-aminophenyl)acetamide for **1b**, or *tert*-butyl (2-aminophenyl)carbamate for **1c**) in the presence of either trifluoroacetic acid (**1a**) or *para*-toluenesulfonic acid monohydrate (*p*TSA, **1b-c**). The synthesis of the dialdehyde precursor was previously reported by Love *et al.*, [64] using diphenyldipyrromethane as a starting material (the synthesis of which was described by Freckmann *et al.*) [65]. In addition, the syntheses of *N*-(2-aminophenyl)acetamide [66] and *tert*-butyl (2-aminophenyl)carbamate [67] are known in the literature. The calixpyrrole ligands **1a** and **b** were obtained as orange or yellow solids, respectively, in moderate yields (60–62 %), whereas **1c** gave much poorer yields overall (26 %). We attributed this lower yield to the Boc protecting groups, which enhanced the solubility of the calixpyrrole ligand in organic solvents.

As mentioned above, **1b** and **1c** were prepared using *p*TSA, following a procedure very similar to the one used by Love and co-workers to generate calixpyrrole "pacman" ligands [38]. This synthetic route was extremely straightforward as the ligands precipitated cleanly from the methanol solvent. For **1a**, on the other hand, this approach also generated the desired product, but the ligand remained soluble in methanol and could not be separated from unwanted side-products (purification via silica gel chromatography was unsuccessful as the calixpyrrole ligand was sensitive to the acidic silica). Following a procedure similar to the one used by Trofimov *et al.* [68], however, **1a** could be synthesized and cleanly isolated. This route utilized trifluoroacetic acid as the catalyst, as well as a concentrated dimethyl sulfoxide reaction mixture. By carefully limiting reaction times, the generation of unwanted side products could be avoided.

The ^{1}H NMR spectra of **1a-c** displayed several characteristic peaks that confirmed the proposed calixpyrrole species had been generated.

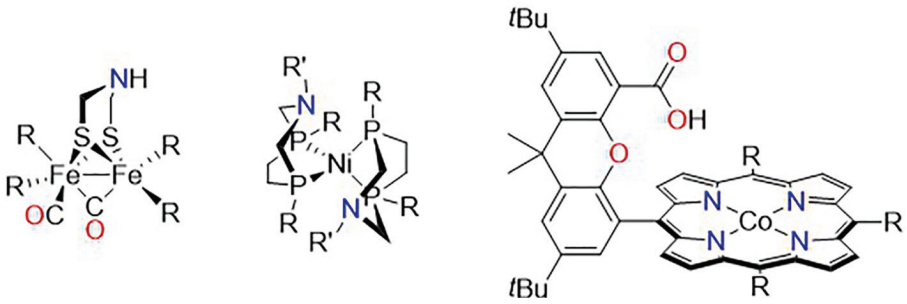

Fig. 1. General structure of diiron azadithiolate-bridged complexes (left), nickel diphosphacycloheptane complexes (middle), and "hangman" porphyrin complexes (right).

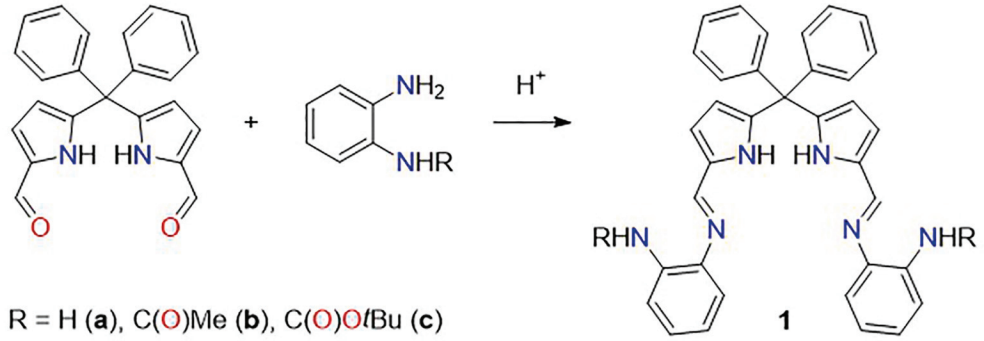

Scheme 1. General Synthetic Procedure for Calixpyrrole Ligands **1a-c**.

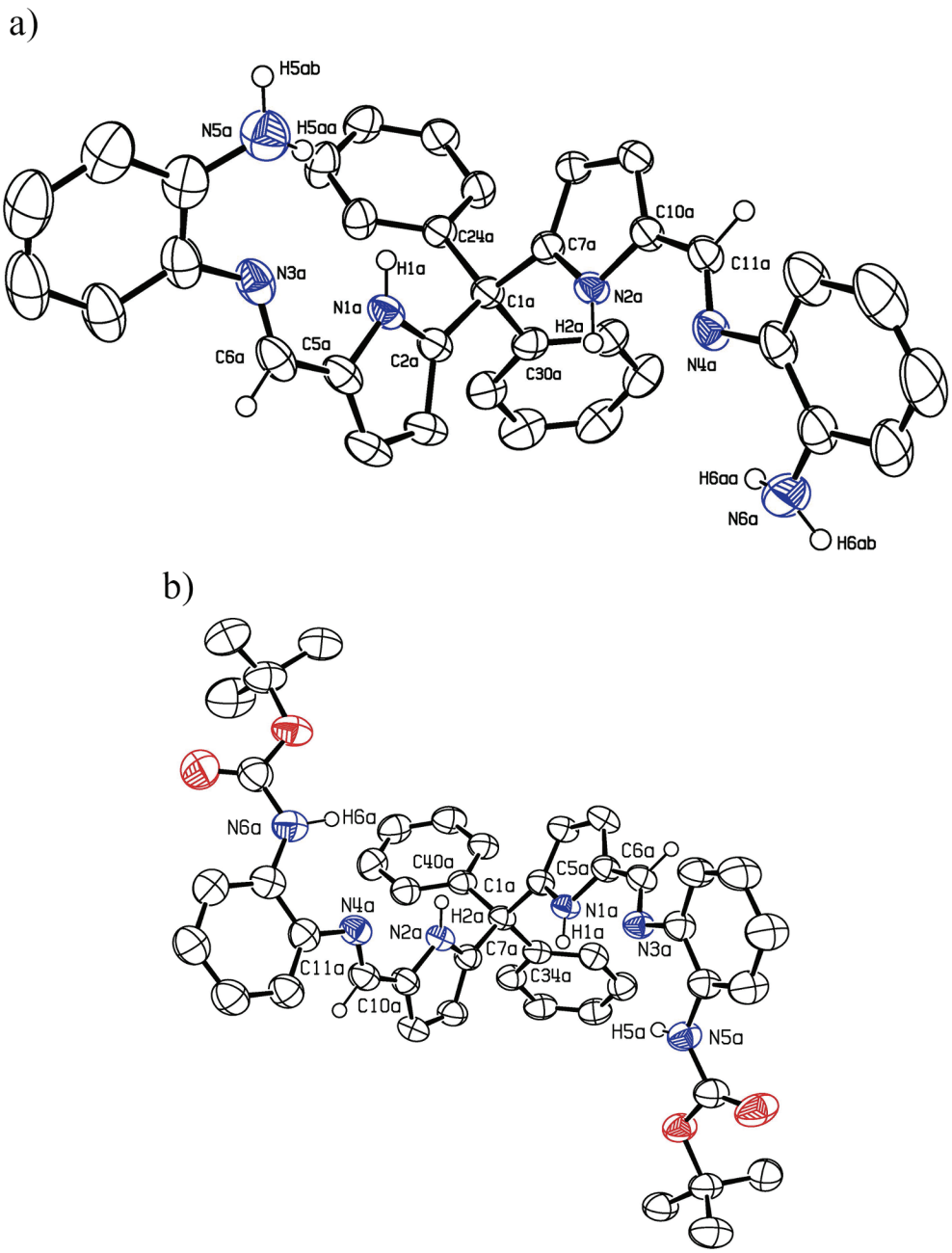

Fig. 3. ORTEP3 representation (thermal ellipsoids at 50% probability) and atom numbering for: a) A single molecule of **1a**, the solvent, most of the hydrogens, and three other molecules of **1a** have been omitted for clarity; b) A single molecule of **1c**, the solvent, most of the hydrogens, and the other molecule of **1c** have been omitted for clarity.

For all three ligands a single imine peak was present in the expected region between 8 and 9 ppm. In addition, when utilizing DMSO-d_6 as the NMR solvent, the NH groups of the pyrrole moieties were visible between 11.36 and 11.46 ppm, as were the pyrrole methine protons between 5.79 and 6.80 ppm. The most characteristic peaks, however, arose from the hydrogens on the arene rings linking the pendant groups to the calixpyrrole ligand framework (between 6.5 and 8.2 ppm). All four of these protons had distinct chemical environments, unlike the symmetric calixpyrrole ligands developed by Love [38] and Sessler [69]. It should also be noted that compounds **1b** and **1c** displayed additional characteristics with the Boc- and acyl-NH peaks visible at 8.22 and 9.26 ppm, respectively, in conjunction with prominent singlets at 1.43 (methyl) and 1.98 ppm (*tert*-butyl), respectively. In contrast, for **1a** a broad singlet indicative of the pendant NH_2 was apparent at 5.28 ppm.

In addition to NMR experiments, compounds **1a-c** were characterized in the solid state utilizing single crystal X-ray diffraction. Crystals of both **1a** and **1c** (Fig. 3) were grown under similar conditions (cold ether), and formed intertwined dimers in the solid state with intermolecular hydrogen bonding between the pyrrole hydrogens, the imine nitrogens, and the hydrogens from the pendant groups (NH_2 for **1a** and Boc-NH for **1c**; for additional ORTEP3 representations of **1a** and **1c** see Fig. A7 Appendix A. Supplementary Data). On average, the dimer of **1a** was more tightly bound together than the dimer of **1c**, most likely due to the bulkier Boc groups in **1c**. There also appeared to be some degree of intermolecular π-π stacking between the arene backbone of one ligand and the phenyl substituent of another (centroid distances between 3.94 and 4.47 Å for **1a**, as well as 3.75 and 3.96 Å for **1c**), which could have provided some driving force for dimer formation (although this could also be due to crystal packing effects due to the relatively long centroid distances). For the unprotected ligand, **1a**, hydrogen bonding interactions between adjacent dimers were also seen: 2.97 and 3.04 Å for H5d–N5a and H5a–N5d (3.39 Å for N5a–N5d), respectivley (for additional hydrogen bond distances see Appendix A. Supplementary Data).

Crystals of **1b**, on the other hand, were not forthcoming using the same conditions as **1a** and **1c**. Instead, a different solvent system (THF layered with pentane) was needed to grow single crystals. As such, **1b** did not form dimers in the solid state (Fig. 4); a single molecule of **1b** was present in the aymmetric unit, which displayed hydrogen bonding to a THF solvent molecule: 2.15 and 2.59 Å for H2–-O1s and H6–O1s (3.02 and 3.33 Å for N2–-O1s and N6–O1s), respectivley. It is not entirely clear at this time why a dimeric species of **1b** did not form in the solid state, but steric factors can likely be ruled out as an acyl protecting group is less sterically demanding than a Boc protecting group. It is possible that hydrogen bonding to THF solvent molecules, which was apparent in the crystal structure of **1b**, disrupted dimer formation as the crystals grew. When comparing **1b** to **1a** and **1c**, many of the bond lengths and angles were very similar, although the N(3)-C(6)-C(5) and N(4)-C(11)-C(10) bond angles for **1b** were slightly closer to the ideal bond angle of 120° (for notable bond lengths and angles for **1a-c** see Table 1).

The synthetic route used to generate the calixpyrrole species **1a-c** is particularly attractive due to its straightforward and modular nature (Scheme 1). A range of aniline precursors were tolerated, including *ortho*-phenylenediamine (with an electron donating NH_2 group) and *N*-(2-aminophenyl)acetamide (with an electron withdrawing $C(O)CH_3$ group). Surprisingly, based on the results seen for the Boc-protected systems, the use of acid-sensitive functionalities was not precluded despite the need for a strong acid to facilitate imine bond formation. Additionally, fairly large functionalities could be incorporated *ortho* to the imine bond (Boc-NH), suggesting that the Schiff-base reaction was relatively insensitive to steric encumbrance in this position. As such, it is hypothesized that starting materials with mono- and di-substituted amines *ortho* to the aniline moiety can be utilized, as well as a range of electron-donating substituents in the *meta* and *para* positions. Electron-withdrawing groups will likely be tolerated as well, but systems that are too electron-poor may cause imine bond-formation to become sluggish. These types of modifications could be extremely useful in future studies for tuning the pK_a values of the pendant groups, as well as the electron donating ability of the imine moieties.

With respect to the 5,5′-diformyldipyrromethane starting material, it is likely that the general synthetic procedure outlined in Scheme 1 will tolerate a range of dialdehyde precursors. Several analogues of these species are known in the literature with alkyl and aryl substituents between the pyrrole donors [38–48]. Substitutions in these positions would offer a useful site to adjust the steric encumbrance of the targeted systems.

Table 1
Selected Bond Lengths (Å) and Angles (deg) for 1a-c.

	1a	1b	1c
	Bond Lengths (Å)		
N(3)/(3A)-C(6)/(6A)	1.275(6)	1.278(6)	1.285(9)
N(4)/(4A)-C(11)/(11A)	1.287(4)	1.278(5)	1.282 (9)
	Bond Angles (deg)		
N(3)/(3A)-C(6)/(6A)-C(5)/(5A)	122.0(3)	121.6(4)	126.2(6)
N(4)/(4A)-C(11)/(11A)-C(10)/(10A)	124.5(3)	121.8(4)	127.1(6)

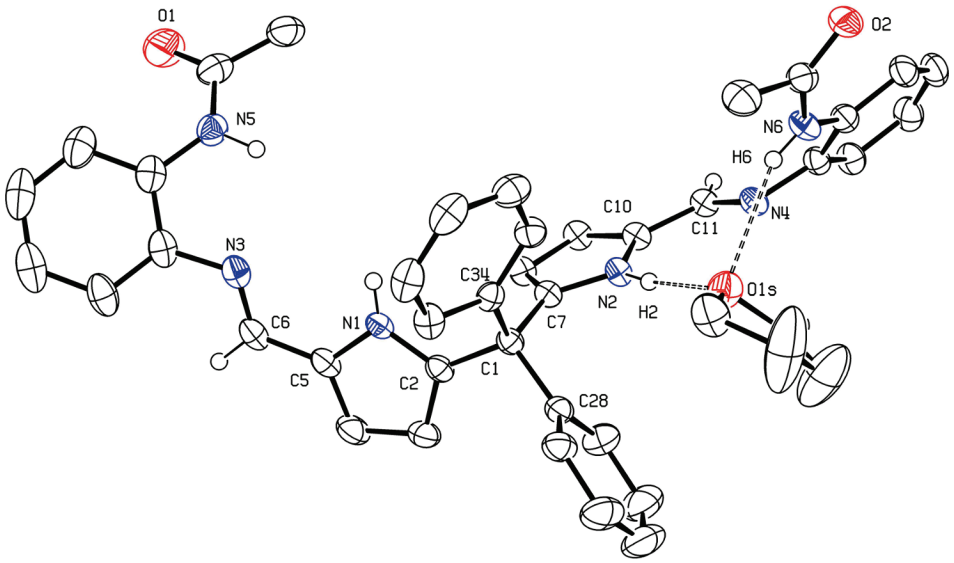

Fig. 4. ORTEP3 representation (thermal ellipsoids at 50% probability) and atom numbering for **1b** where most of the hydrogen have been omitted for clarity.

2.2. Synthesis and characterization of compounds 2a-c

In order to probe the binding modes of **1a-c** the calixpyrrole ligands were coordinated to palladium(II) and the resulting complexes were characterized. Palladium(II) was chosen in order to generate diamagnetic species, which would aid with spectroscopic characterization, and because palladium complexes with pendant nitrogen-based groups have been shown to electrocatalytically reduced oxygen [20]. The pyrrole species were first deprotonated with two equivalents of KH, followed by a salt metathesis reaction with one equivalent of $Pd(OAc)_2$ to give four coordinate square planar complexes, **2a-c** (Scheme 2). These compounds could be isolated as red (**2a**) or orange (**2b-c**) solids in moderate to good yields (35–57 %).

The ^{1}H NMR spectra of compounds **2a-c** all showed characteristic peaks that were shifted from the free ligand forms. In particular, a significant upfield shift of the imine C—H signals was seen, with peaks at 7.75, 7.55, and 7.60 ppm for **2a**, **2b**, and **2c**, respectively. Moreover, the absence of the pyrrole NH signals between 11 and 12 ppm indicated that the calixpyrrole ligands had been successfully deprotonated in the desired positions. This was in contrast to the pendant groups, which still displayed NH peaks at 4.45, 7.65, and 8.33 pm for **2a**, **2b**, and **2c**, respectively. In addition to NMR spectroscopy complexes **2a-c** were all characterized in the solid state utilizing single crystal X-ray diffraction (Fig. 5). In all three structures the palladium centres adopted distorted square planar coordination geometries with the metal bound slightly out of the plane of the four nitrogen donors (0.08, 0.06, and 0.02 Å for **2a**, **2b**, and **2c**, respectively). In addition, the metal centre was found to sit closer to the pyrrolide nitrogens, consistent with the results reported by Love *et al.* [38] for bimetallic palladium "pacman" complexes. This distortion was reflected in the shorter Pd(1)-N(1) and Pd(1)-N(2) bond lengths (1.947(9) and 1.951(9) Å for **2a**, 1.945(4) and 1.938(4) Å for **2b**; 1.941(6) and 1.940(6) Å for **2c**) in comparison to longer Pd(1)-N(3) and Pd(1)-N(4) bond lengths (2.086(9) and 2.080(9) Å for **2a**; 2.080(4) and 2.0999(4) Å for **2b**; 2.075(6) and 2.065(6) Å for **2c**). The bond angles for the palladium species were also consistent with previous findings for palladium-based "pacman" complexes [38]. The N(1)-Pd(1)-N(2) bond angle between the pyrrolide donors was only slightly compressed below 90°, while the N(1)-Pd(1)-N(3) and N(2)-Pd(1)-N(4) bond angles were significantly smaller. This can be attributed to the five membered rings that formed between the imine, pyrrolide, and palladium centre upon coordination (the N(3)-C(6)-C(5) and N(4)-C(11)-C(10) imine bond angles were also compressed in comparison to the free ligands). In order to compensate for all of the other metal–ligand bond angles, the N(3)-Pd(1)-N(4) bond angle was expanded above 90° (110.6(4), 112.2(2), and 110.6(2)° for **2a**, **2b**, and **2c**, respectively). Interestingly, the imine bond lengths (C(6)-N(3) and C(11)-N(4)) increased by 0.029 Å on average upon coordinating a metal centre suggesting that some degree of back-bonding was occurring from the palladium. This hypothesis was supported by density functional theory (DFT) calculations, which showed a molecular orbital (HOMO-10) with significant d-orbital character on the metal centre and antibonding character on the imine donors (see Fig. A8 in Appendix A. Supplementary Data for a visualization of this orbital). For other notable bond lengths and angles see Table 2.

With respect to the pendant groups, no interaction with the metal centre was apparent in the solid state, as indicated by the Pd(1)-N(5) and Pd(1)-N(6) distances of 3.49 and 3.52 Å for **2a**, 3.36 and 4.79 Å for **2b**, as well as 3.61 and 3.47 Å for **2c**. These moieties are likely close enough, however, to interact with a ligand bound in an axial coordination site. The large asymmetry in values seen for the acyl-protected species was caused by hydrogen bonding (2.18 Å for H(5)–O(2) and 2.97 Å for N(5)–O(2)) between the adjacent amide moieties, which oriented N(6) further away from the metal centre. Additionally, the intramolecular interaction caused both pendant groups to align on the same side of the palladium complex. In **2a** and **2c**, on the other hand, no hydrogen bonding was seen and the pendant groups were located on opposite sides of the calixpyrrole ligand. In solution, however, the pendant groups can freely rotate as determined by NMR spectroscopy.

2.3. Electrochemical properties of 1–2

The electrochemical properties of compounds **1a-c** and **2a-c** in acetonitrile were evaluated using cyclic voltammetry (CV) with tetrabutylammonium hexafluorophosphate (TBAP) as the supporting electrolyte (Fig. 6). The acyl- and Boc-protected ligands showed similar features: an irreversible oxidation at higher potentials (around 1.22 and 1.27 V vs ferrocene/ferrocenium, Fc/Fc^+, for **1b** and **1c**, respectively) and two irreversible reductions at lower potentials (-1.04 and −1.61 V for **1b**, as well as −1.04 and −1.71 V for **1c**). The Boc-protected system, however, exhibited an additional oxidation and reduction at 0.07 and −0.01 V, respectively. The unprotected ligand, **1a**, on the other hand, had two irreversible oxidations at 0.07 and 0.74 V vs Fc/Fc^+, as well as two irreversible reductions at −1.09 and −1.74 V. With respect to the palladium complexes, they all produced analogous features to one another: two irreversible oxidations seen at higher potentials and two irreversible reductions seen at lower potentials. For **2b** and **2c** the irreversible reductions and oxidations occurred at very similar potentials (-1.42, −0.8, 0.45, and 0.84 V for **2b**; −1.34, −0.99, 0.47, and 0.82 V for **2c**), but for **2a** they occurred at lower potentials (0.08 and 0.58 V for the oxidations and −1.10 and −1.64 V for the reductions). When comparing the CVs of **1a-c** and **2a-c** it is clear that the ligands are redox non-innocent, and that the locations of the irreversible oxidations and reductions were only shifted somewhat upon metal coordination.

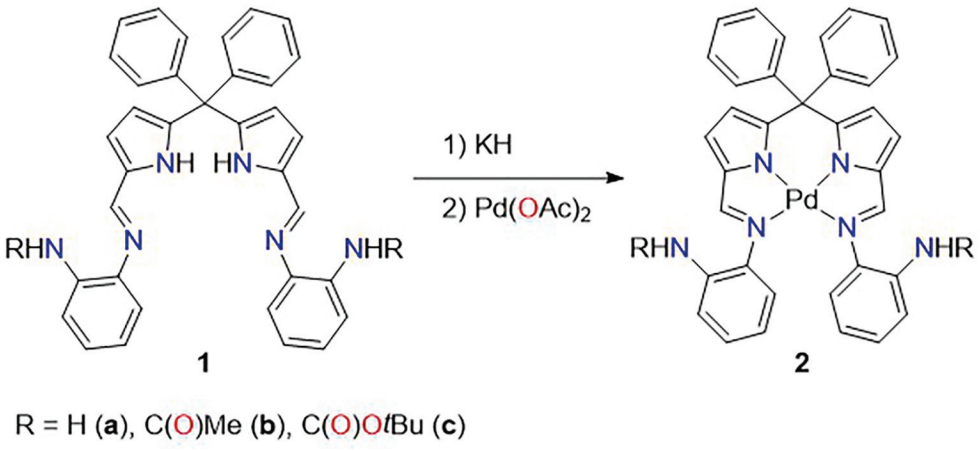

Scheme 2. General Synthetic Procedure for Palladium Complexes **2a-c**.

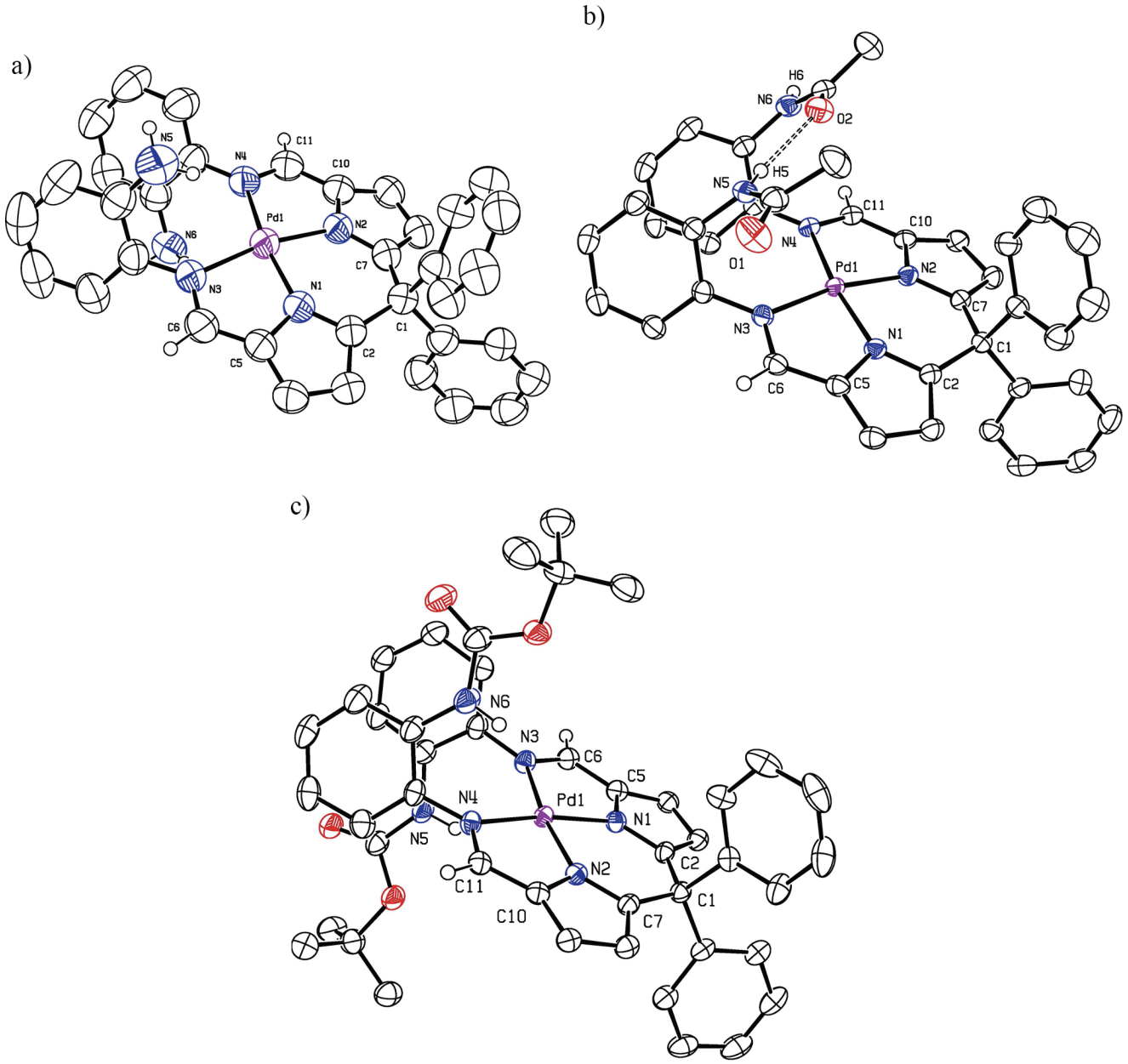

Fig. 5. ORTEP3 representation (thermal ellipsoids at 50% probability) and atom numbering for: a) **2a**, most of the hydrogens have been omitted for clarity; b) **2b**, the solvent and most of the hydrogens have been omitted for clarity; c) **2c**, the solvent and most of the hydrogens have been omitted for clarity.

Table 2
Selected Bond Lengths (Å) and Bond Angles (deg) for 2a-c.

	2a	2b	2c
	Bond Lengths (Å)		
Pd(1)-N(1)	1.947(9)	1.945(4)	1.941(6)
Pd(1)-N(2)	1.951(9)	1.938(4)	1.940(6)
Pd(1)-N(3)	2.086(9)	2.080(4)	2.075(6)
Pd(1)-N(4)	2.080(9)	2.099(4)	2.065(6)
N(3)-C(6)	1.31(2)	1.308(6)	1.313(9)
N(4)-C(11)	1.30(2)	1.314(6)	1.317(9)
	Bond Angles (deg)		
N(1)-Pd(1)-N(2)	87.9(4)	88.0(2)	88.2(2)
N(1)-Pd(1)-N(3)	80.7(4)	79.8(2)	80.6(2)
N(2)-Pd(1)-N(4)	80.4(4)	79.8(2)	80.7(2)
N(3)-Pd(1)-N(4)	110.6(4)	112.2(2)	110.6(2)
N(3)-C(6)-C(5)	119(1)	117.5(4)	118.4(6)
N(4)-C(11)-C(10)	119(1)	118.3(4)	118.3(6)

From the CV experiments it is also apparent that the unprotected compounds **1a** and **2a** behaved somewhat differently than their corresponding Boc- and acyl-protected analogues. In particular their irreversible reduction and oxidations occurred at lower potentials in comparison to **1b**, **1c**, **2b**, and **2c**. Deprotonation of the pendant NH_2 groups upon oxidation can be ruled out, however, as the addition of triethylamine or pyridine did not shift these irreversible oxidations to more reducing potentials, and did not induce an increase in peak current. Instead, the more electron-rich nature of **1a** and **2a** can be rationalized by the increased electron-donating ability of the aniline moieties in comparison to acetamide and carbamate functionalities.

2.4. Theoretical calculations

In order to assign the CVs of **2a-c**, DFT calculations utilizing the B3LYP functional and 6-311++G** (H, C, N) + Def2-TZVP + ECP (Pd) basis sets were performed. A model system with pendant NH_2 groups on

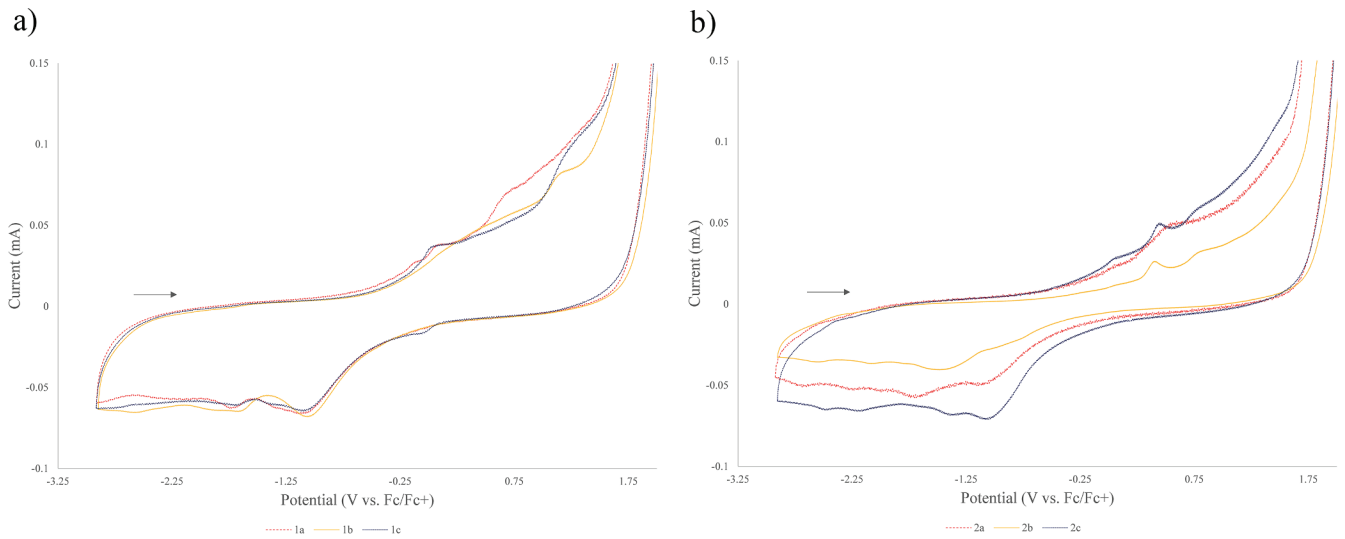

Fig. 6. Cyclic voltammograms in acetonitrile (0.25 mM ligand or complex, 0.1 M TBAP, glassy carbon working electrode, platinum wire counter electrode, 0.01 M $Ag/AgNO_3$ reference electrode, scan rate = 800 mV/s) of: a) **1a-c**; b) **2a-c**.

the aryl backbone and hydrogen atoms in place of the phenyl groups between the pyrrole moieties (to reduce computational cost) was used. Ground state optimizations and frequency calculations were carried out for neutral ($\mathbf{2a_H}$) and cationic ($\mathbf{2a_H^+}$ and $\mathbf{2a_H^{2+}}$) species. For $\mathbf{2a_H^{2+}}$ both open- (S = 1) and closed-shell (S = 0) states were calculated, with the S = 1 state being lower in energy by 7.3 kcal/mol (further discussions below for $\mathbf{2a_H^{2+}}$ will refer to the S = 1 state).

When examining the HOMO, HOMO-1, and HOMO-2 orbitals of $\mathbf{2a_H}$ they were mainly ligand-based with very little metal d-character (Fig. 7). For the charged species shown in Fig. 7: in $\mathbf{2a_H^+}$ the SOMO had significant ligand character (similar in character to the HOMO-1 in $\mathbf{2a_H}$) and in $\mathbf{2a_H^{2+}}$ the both SOMOs were mostly ligand-based (similar in character to the HOMO and HOMO-1 in $\mathbf{2a_H}$, respectively). These results suggested that in all of the complexes examined, the Pd centre stayed in the + 2 oxidation state, and that electrons were removed from mainly ligand-based orbitals upon oxidation. This was also reflected in the Mulliken charge on the metal in $\mathbf{2a_H}$, $\mathbf{2a_H^+}$, and $\mathbf{2a_H^{2+}}$: 1.71, 1.54, and 1.46, respectively.

Therefore, the DFT calculations indicated that all of the oxidations seen in the CVs of **2a-c** were mainly ligand-based. This matched well with the experimental data, as the CVs of **1a-c** and their corresponding metal complexes were very similar. Additionally, pyrrole groups are known to be prone to oxidation, which would explain the redox non-innocence seen for the calixpyrrole ligands [70]. What is particularly striking about these results, however, is that they suggest a total of two electrons could be removed from the calixpyrrole ligand without greatly affecting the oxidation state of the metal centre. Looking at the orbitals shown in Fig. 7, this is likely facilitated by the extensive conjugation across the whole ligand, which would prevent the build-up of localized charge. As such, the calixpyrrole ligands **1a-c** displayed redox non-innocence somewhat similar to porphyrin ligands, except that the oxidized forms of **1a-c** were much less stable (leading to the mainly irreversible electrochemistry observed). This is encouraging when considering the calixpyrrole species for small molecule activation studies as the ligands themselves can act as an electron reservoir and delocalize charge across the whole molecule. Lastly, with respect to the two irreversible reductions seen in the CVs of **2a-c**, it is believed that these were mainly metal-based reductions. This hypothesis was also supported by the theoretical calculations that were performed, in that the LUMO of $\mathbf{2a_H}$ displayed significant metal d-orbital character (see Fig. A8 in Appendix A. Supplementary Data for a visualization of this orbital).

2.5. Preliminary small molecule reactivity studies

Preliminary binding studies utilizing **2a-c** and O_2, H_2O, N_2, NH_3, H_2, CO_2, and MeOH indicated that there was little to no interaction with the neutral palladium complexes at room temperature. This was perhaps to be expected given the square planar binding mode of palladium and the Jahn-Teller distortions that would disfavour ligand binding in the axial positions. The CVs of **2a-c** in the presence of various substrates were also carried out to examine the potential reactivity of the calixpyrrole complexes. No catalytic currents were observed under an N_2, O_2, or CO_2 atmosphere in the presence of various acids (lutidinium tetrafluoroborate or trifluoroacetic acid), nor were they observed under an H_2 or NH_3 atmosphere or with MeOH and/or H_2O in the presence of various bases (triethylamine, lutidine, or pyridine).

When examining the CV data and the electronic structure of $\mathbf{2a_H}$, the reasons for the lack of reactivity displayed by **2a-c** under the reaction conditions that were explored become apparent. Based on the reduction potentials of the palladium species, they are more likely to engage in reduction reactions than oxidation reactions. The DFT calculations, however, showed that the HOMO to HOMO-3 orbitals were all mainly ligand-based, with the HOMO-4, HOMO-5, HOMO-6, HOMO-8, HOMO-9, HOMO-10, and HOMO-11 orbitals displaying more significant metal character (see Fig. A8 in Appendix A. Supplementary Data for visualizations of these orbitals). It is likely that the metal-based orbitals are too low in energy to facilitate electron transfer from Pd(II) to a substrate of interest. This hypothesis was supported by the results reported herein, where upon oxidation (as discussed above), the frontier orbitals remained mainly ligand-based and the electrochemistry of **2a-c** was mostly irreversible.

Although the palladium complexes were not able to activate the small molecules that were investigated, we still view the calixpyrrole species **1a-c** as promising ligand frameworks. The amount of control over the secondary coordination sphere enabled by these calixpyrrole architectures should provide an avenue for facilitating PCET, and the high degree conjugation across the ligand structure is anticipated facilitate electron transfer reactions. It is clear, however, that increased metal d-orbital character in the HOMO to HOMO-3 orbitals will be crucial in order to get the metal centre involved in redox processes and lead to more desirable electrochemical properties (reversible redox couples). More studies are needed to explore alternative metals and different coordination geometries using ligands **1a-c**.

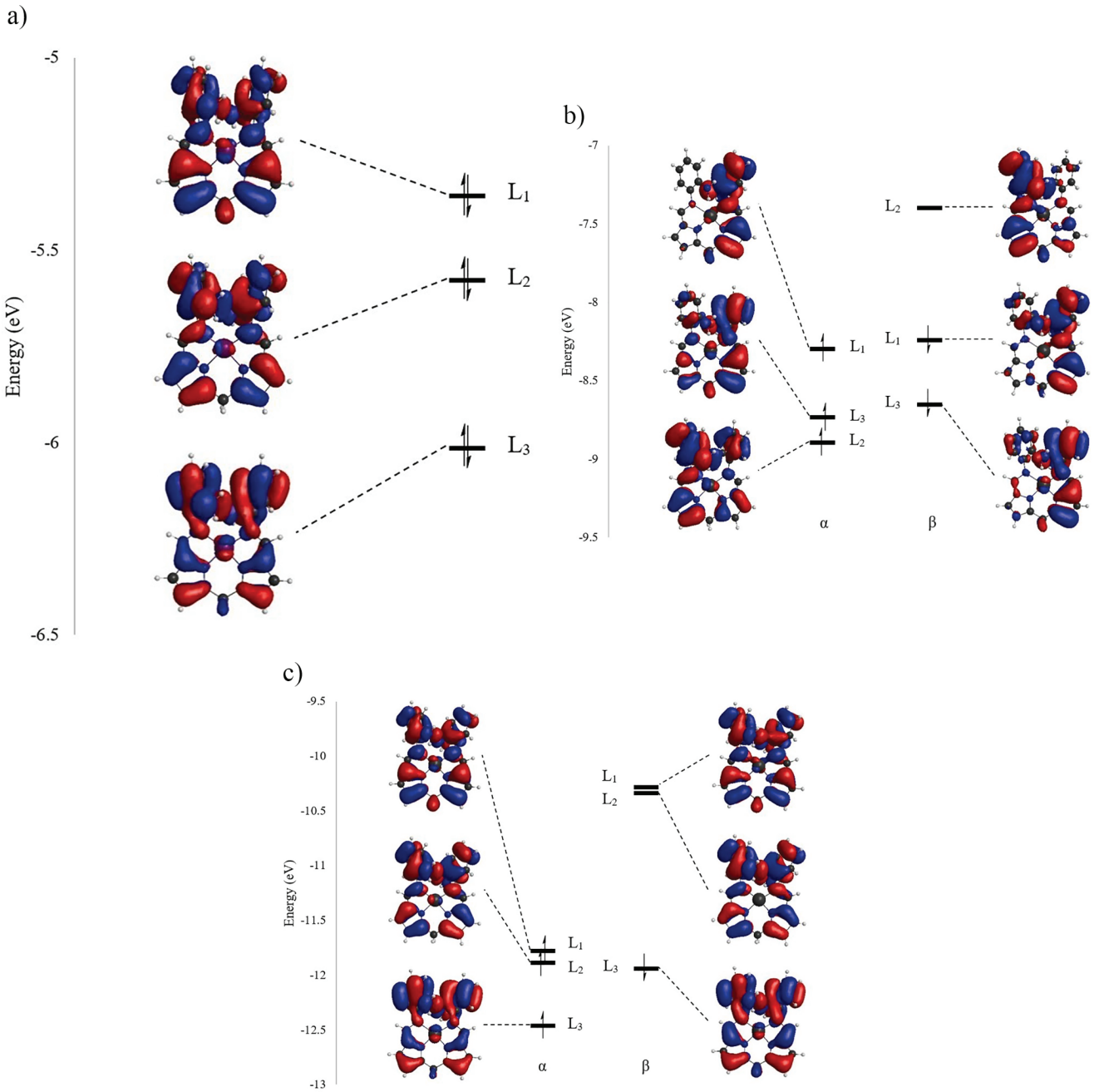

Fig. 7. Visual representations and energies of the a) ligand-based HOMO, HOMO-1, HOMO-2 orbitals (labelled L_1, L_2, and L_3, respectively) of $\mathbf{2a_H}$; b) ligand-based HOMO, HOMO-1, and HOMO-2 (SOMO) orbitals of $\mathbf{2a_H}^+$ (α and β manifolds, labelled L_1, L_3, and L_2, respectively, in reference to the orbitals with similar character in $\mathbf{2a_H}$); c) HOMO (SOMO), HOMO-1 (SOMO), and HOMO-2 orbitals of $\mathbf{2a_H}^{2+}$ with S = 1 (α and β manifolds, labelled L_1, L_2, and L_3, respectively, in reference to the orbitals with similar character in $\mathbf{2a_H}$).

2.6. *Electrocatalytic H_2 evolution*

While the palladium complexes **2a-c** did not engage in small molecule activation under the conditions outlined above, they did exhibit electrocatalytic H_2 production in the presence of a strong acid: *p*TSA (Fig. 8). The onset of catalysis for **2a-c** was approximately 0.4–0.5 V more positive than the glassy carbon electrode itself (between − 0.65 V to 0.71 V for **2a-c**, and – 1.08 V for the glassy carbon electrode) and the peak current varied linearly with the square root of the scan rate (see Figs. A9–A11 in Appendix A. Supplementary Data). The catalytic peak did shift to more negative potentials at higher scan rates, however, and the nature of the ligand (**a-c**) did not seem to have a significant impact on catalysis under the conditions that were examined (using 600 equivalents of a strong acid *p*TSA). These results suggested that hydrogen evolution was limited by diffusion of protons to the electrode surface and that the active catalytic species was heterogeneous in nature. This was confirmed upon performing a "rinse" test: [71] after carrying out electrocatalysis in a 0.25 mM solution of **2a-c** in acetonitrile (0.1 M TBAP and 0.15 M *p*TSA), the working electrode was gently rinsed in a 0.1 M TBAP solution in acetonitrile, and then submerged in a fresh acetonitrile solution without any palladium complex (0.1 M TBAP and 0.15 M *p*TSA). It was found that H_2 production still proceeded in the absence of palladium complex in the bulk solution (up to 100 cycles without significant changes in activity), indicating that the active catalyst was supported on the working electrode surface (see Figs. A12–A14 in Appendix A. Supplementary Data). Moreover, after

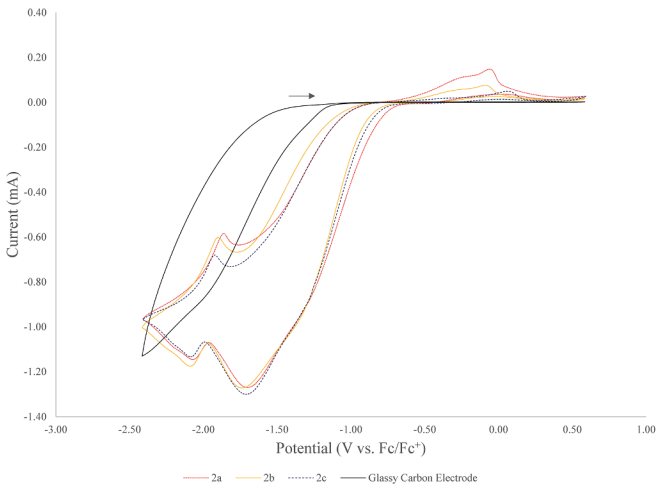

Fig. 8. Cyclic voltammograms in acetonitrile (0.25 mM complex, 0.1 M TBAP, glassy carbon working electrode, platinum wire counter electrode, 0.01 M Ag/$AgNO_3$ reference electrode, scan rate = 100 mV/s) of **2a-c** in the presence of 600 equivalents of *p*TSA (0.15 M).

electrocatalysis the working electrode was visually no longer "glassy" (suggesting the formation of a heterogeneous species).

Due to the redox non-innocent nature of ligands **1a-c**, control experiments investigating the catalytic abilities of the free calixpyrrole species were carried out (see Fig. A15 in Appendix A. Supplementary Data for a representative example). The non-coordinated ligand species did not catalyze H_2 production, demonstrating that palladium was crucial for this transformation. Moreover, CV experiments were carried out in deuterated acetonitrile to verify that the effervescence seen at the working electrode was due to H_2 evolution. A characteristic H_2 peak around 4.56 ppm was observed (see Fig. A16 in Appendix A. Supplementary Data) supporting that the catalytic currents displayed in the CVs of **2a-c** were due to H_2 production. Interestingly, the active species were fairly robust, undergoing over 500 scans without significant changes in the CV features (see Fig. A17 in Appendix A. Supplementary Data).

Based on all of the observations outlined above (both experimental and theoretical), it is believed that reduction of palladium in **2a-c** (corresponding to the first irreversible reduction seen around −0.8 to −1.10 V in Fig. 6) under acidic conditions forms the active catalytic species, which is heterogeneous in nature. Once the active species initially forms on the electrode surface, it does not appear that further reactions with **2a-c** in solution are necessary for catalytic activity (as shown by the "rinse" test studies). Furthermore, the active catalyst does not seem to react further with **2a-c** in solution over the course of 500 scans under catalytic conditions (or if it does, this does not change the activity and electrochemical properties of the catalytic site significantly). It is hypothesized that the working electrode becomes innervated with respect to reaction with palladium species in solution after catalyst formation, potentially by a thin film (caused by electropolymerization of the porphyrin-like calixpyrrole ligand) [72] that prevents further deposition of **2a-c**. If clusters or nanoparticles are formed, they are likely stabilized by the calixpyrrole ligand, or possibly-one of its decomposition products. Additionally, if the catalyst is a nanoparticle species, the active catalytic surface area does not change appreciably over 500 cycles of use. These results are particularly exciting because they suggest only a small amount of the palladium in solution is needed to generate a robust catalytic system for H_2 evolution.

Due to the heterogeneous nature of the active catalyst, however, very different methods are needed to characterize this species in comparison to those outlined for the homogeneous compounds **1a-c** and **2a-c**. As such, further studies are needed to identify the exact nature of the heterogeneous catalyst (i.e. whether thin films, small clusters, or larger nanoparticles are formed), before a proper kinetic analysis of these systems can be carried out (determining turnover frequencies, faradaic efficiencies, etc.). These investigations will be the subject of a future publication, and are currently underway.

3. Conclusion

In summary, a series of calixpyrrole ligands with pendant nitrogen-based functionalities, **1a-c**, were synthesized using a modular Schiff-base reaction starting with either commercially available or easily accessible starting materials. The hydrogen bond donors in the secondary coordination sphere could be readily varied, and a wide range of aniline precursors could be utilized, including species with amino, amide, and carbamate substituents. This was particularly attractive as the pendant groups could be easily tuned, which could provide a high degree of control over the secondary coordination sphere in future studies. In order to investigate the binding modes of these tetradentate ligands, they were coordinated to palladium generating square planar complexes **2a-c**. No interaction was observed between the metal centre and the pendant groups in the solid state, but structures with both hydrogen bond donors on the same side of the calixpyrrole ligand, as well as on opposite sides of the calixpyrrole ligand, were seen. Interestingly, the nitrogen-based substituents in the secondary coordination sphere seemed well positioned to interact with ligands binding in the axial coordination sites, indicating that they could potentially activate substrates and facilitate PCET under the right conditions. In addition, the electrochemical properties of **1**–**2** were explored. The calixpyrrole ligands were found to be redox non-innocent, and theoretical studies suggested that up to two electrons could be removed from the ligand system without affecting the oxidation state of the palladium centre. This was likely facilitated by extensive conjugation across the calixpyrrole species; a property which could potentially be leveraged for multi-electron transfer processes. Lastly, although oxidations were seen at potentials relevant for small molecule activation, **2a-c** were found to be unreactive towards a variety of small molecule substrates. Based on preliminary binding studies, it is believed that Jahn-Teller distortions disfavoured substrate binding to the square planar palladium complexes. Moreover, theoretical calculations suggested that the metal-based orbitals were too stabilized to properly engage in redox processes. Despite the initial lack of reactivity seen with **2a-c**, they were found to generate systems that could catalyze H_2 evolution in the presence of *p*TSA. The onset of electrocatalysis was around 0.4–0.5 V more positive than the glassy carbon working electrode, and the catalysts were stable for over 500 scans with no signs of deactivation. The catalytically active species were found to be heterogeneous in nature, and affected H_2 production in the absence of palladium complex in the bulk solution. Further studies exploring these exciting ligand frameworks and heterogeneous H_2 evolution electrocatalysts are currently Underway.

CRediT authorship contribution statement

Logan Trowbridge: Methodology, Validation, Formal analysis, Investigation, Writing – original draft, Visualization. **Boris Averkiev:** Formal analysis, Investigation, Data curation, Visualization. **Peter E. Sues:** Conceptualization, Methodology, Formal analysis, Validation, Investigation, Resources, Data curation, Writing – original draft, Writing – review & editing, Visualization, Supervision, Project administration, Funding acquisition.

Declaration of Competing Interest

The authors declare that they have no known competing financial interests or personal relationships that could have appeared to influence the work reported in this paper.

Data availability

Data will be made available on request.

Acknowledgements

This work was supported by the National Science Foundation (grant numbers CHE-2018414 and CHE-1826982) which provided funding used to purchase the single-crystal X-ray diffractometer and associated software employed in this study, as well as the Bruker 400 MHz spectrometer. We would also like to thank Dr. William Brennessel from the CENTC Elemental Analysis Facility at the University of Rochester for performing the elemental analyses.

Appendix A. Supplementary data

Supplementary data to this article can be found online at https://doi.org/10.1016/j.poly.2022.116046.

References

[1] bp Statistical Review of World Energy 2020; 69th Edition; BP p.l.c.: London, UK, June 17, 2020, 1-65.
[2] F. Barbir, T.N. Veziroğlu, H.J. Plass, Environmental Damage Due to Fossil Fuels Use, Int. J. Hydrog. Energy 15 (10) (1990) 739–749, https://doi.org/10.1016/0360-3199(90)90005-J.
[3] L. Al-Ghussain, Global Warming: Review on Driving Forces and Mitigation, Environ. Prog. Sustain. Energy 38 (1) (2019) 13–21, https://doi.org/10.1002/ep.13041.
[4] D.K. Bediako, B.H. Solis, D.K. Dogutan, M.M. Roubelakis, A.G. Maher, C.H. Lee, M. B. Chambers, S. Hammes-Schiffer, D.G. Nocera, Role of Pendant Proton Relays and Proton-Coupled Electron Transfer on the Hydrogen Evolution Reaction by Nickel Hangman Porphyrins, Proc. Natl. Acad. Sci. 111 (42) (2014) 15001–15006.
[5] M.P. Stewart, M.-H. Ho, S. Wiese, M.L. Lindstrom, C.E. Thogerson, S. Raugei, R. M. Bullock, M.L. Helm, High Catalytic Rates for Hydrogen Production Using Nickel Electrocatalysts with Seven-Membered Cyclic Diphosphine Ligands Containing One Pendant Amine, J. Am. Chem. Soc. 135 (16) (2013) 6033–6046, https://doi.org/10.1021/ja400181a.
[6] G. Sahara, O. Ishitani, Efficient Photocatalysts for CO_2 Reduction, Inorg. Chem. 54 (11) (2015) 5096–5104, https://doi.org/10.1021/ic502675a.
[7] Y.J. Jang, A.E. Lindberg, M.A. Lumley, K.-S. Choi, Photoelectrochemical Nitrogen Reduction to Ammonia on Cupric and Cuprous Oxide Photocathodes, ACS Energy Lett. 5 (6) (2020) 1834–1839, https://doi.org/10.1021/acsenergylett.0c00711.
[8] S.-Y. Liu, J.D. Soper, J.Y. Yang, E.V. Rybak-Akimova, D.G. Nocera, Mechanistic Studies of Hangman Salophen-Mediated Activation of O−O Bonds, Inorg. Chem. 45 (19) (2006) 7572–7574, https://doi.org/10.1021/ic0602087.
[9] M. Frey, Hydrogenases: Hydrogen-Activating Enzymes, ChemBioChem 3 (2–3) (2002) 153–160, https://doi.org/10.1002/1439-7633(20020301)3:2/3<153::AID-CBIC153>3.0.CO;2-B.
[10] K.A. Vincent, A. Parkin, F.A. Armstrong, Investigating and Exploiting the Electrocatalytic Properties of Hydrogenases, Chem. Rev. 107 (10) (2007) 4366–4413, https://doi.org/10.1021/cr050191u.
[11] J.C. Fontecilla-Camps, A. Volbeda, C. Cavazza, Y. Nicolet, Structure/Function Relationships of [NiFe]- and [FeFe]-Hydrogenases, Chem. Rev. 107 (10) (2007) 4273–4303, https://doi.org/10.1021/cr050195z.
[12] D.F. Harris, D.A. Lukoyanov, S. Shaw, P. Compton, M. Tokmina-Lukaszewska, B. Bothner, N. Kelleher, D.R. Dean, B.M. Hoffman, L.C. Seefeldt, Mechanism of N_2 Reduction Catalyzed by Fe-Nitrogenase Involves Reductive Elimination of H_2, Biochemistry 57 (5) (2018) 701–710, https://doi.org/10.1021/acs.biochem.7b01142.
[13] B.M. Hoffman, D. Lukoyanov, D.R. Dean, L.C. Seefeldt, Nitrogenase: A Draft Mechanism, Acc. Chem. Res. 46 (2) (2013) 587–595, https://doi.org/10.1021/ar300267m.
[14] S.Y. Reece, D.G. Nocera, Proton-Coupled Electron Transfer in Biology: Results from Synergistic Studies in Natural and Model Systems, Annu. Rev. Biochem. 78 (1) (2009) 673–699, https://doi.org/10.1146/annurev.biochem.78.080207.092132.
[15] J.-M. Savéant, Proton Relays in Molecular Catalysis of Electrochemical Reactions: Origin and Limitations of the Boosting Effect, Angew. Chem. Int. Ed. 58 (7) (2019) 2125–2128, https://doi.org/10.1002/anie.201812375.
[16] R. Tyburski, T. Liu, S.D. Glover, L. Hammarström, Proton-Coupled Electron Transfer Guidelines, Fair and Square, J. Am. Chem. Soc. 143 (2) (2021) 560–576, https://doi.org/10.1021/jacs.0c09106.
[17] O. Lampret, J. Duan, E. Hofmann, M. Winkler, F.A. Armstrong, T. Happe, The Roles of Long-Range Proton-Coupled Electron Transfer in the Directionality and Efficiency of [FeFe]-Hydrogenases, Proc. Natl. Acad. Sci. 117 (34) (2020) 20520–20529, https://doi.org/10.1073/pnas.2007090117.
[18] C. Madden, M.D. Vaughn, I. Díez-Pérez, K.A. Brown, P.W. King, D. Gust, A. L. Moore, T.A. Moore, Catalytic Turnover of [FeFe]-Hydrogenase Based on Single-Molecule Imaging, J. Am. Chem. Soc. 134 (3) (2012) 1577–1582, https://doi.org/10.1021/ja207461t.
[19] K. Pandey, S.T.A. Islam, T. Happe, F.A. Armstrong, Frequency and Potential Dependence of Reversible Electrocatalytic Hydrogen Interconversion by [FeFe]-Hydrogenases, Proc. Natl. Acad. Sci. 114 (15) (2017) 3843–3848, https://doi.org/10.1073/pnas.1619961114.
[20] J.W. Schultz, N.P. Rath, L.M. Mirica, Improved Oxidative C-C Bond Formation Reactivity of High-Valent Pd Complexes Supported by a Pseudo-Tridentate Ligand, Inorg. Chem. 59 (16) (2020) 11782–11792, https://doi.org/10.1021/acs.inorgchem.0c01763.
[21] S. Sinha, L.M. Mirica, Electrocatalytic O_2 Reduction by an Organometallic Pd(III) Complex via a Binuclear Pd(III) Intermediate, ACS Catal. 11 (9) (2021) 5202–5211, https://doi.org/10.1021/acscatal.0c05726.
[22] T.B. Rauchfuss, Diiron Azadithiolates as Models for the [FeFe]-Hydrogenase Active Site and Paradigm for the Role of the Second Coordination Sphere, Acc. Chem. Res. 48 (7) (2015) 2107–2116, https://doi.org/10.1021/acs.accounts.5b00177.
[23] M.L. Helm, M.P. Stewart, R.M. Bullock, M.R. DuBois, D.L. DuBois, A Synthetic Nickel Electrocatalyst with a Turnover Frequency Above 100,000 S^{-1} for H_2 Production, Science 333 (6044) (2011) 863–866, https://doi.org/10.1126/science.1205864.
[24] H.J.S. Brown, S. Wiese, J.A.S. Roberts, R.M. Bullock, M.L. Helm, Electrocatalytic Hydrogen Production by $[Ni(7P^{Ph}_2N^H)_2]^{2+}$: Removing the Distinction Between Endo- and Exo-Protonation Sites, ACS Catal. 5 (4) (2015) 2116–2123, https://doi.org/10.1021/cs502132y.
[25] J.Y. Yang, S. Chen, W.G. Dougherty, W.S. Kassel, R.M. Bullock, D.L. DuBois, S. Raugei, R. Rousseau, M. Dupuis, M.R. DuBois, Hydrogen Oxidation Catalysis by a Nickel Diphosphine Complex with Pendant Tert-Butyl Amines, Chem. Commun. 46 (45) (2010) 8618–8620, https://doi.org/10.1039/C0CC03246H.
[26] J.M. Hodgkiss, A. Krivokapić, D.G. Nocera, Ligand-Field Dependence of the Excited State Dynamics of Hangman Bisporphyrin Dyad Complexes, J. Phys. Chem. B 111 (28) (2007) 8258–8268, https://doi.org/10.1021/jp070447v.
[27] J. Rosenthal, L.L. Chng, S.D. Fried, D.G. Nocera, Stereochemical Control of H2O2 Dismutation by Hangman Porphyrins, Chem. Commun. 25 (2007) 2642–2644, https://doi.org/10.1039/B616884A.
[28] M. Schwalbe, D.K. Dogutan, S.A. Stoian, T.S. Teets, D.G. Nocera, Xanthene-Modified and Hangman Iron Corroles, Inorg. Chem. 50 (4) (2011) 1368–1377, https://doi.org/10.1021/ic101943h.
[29] C.H. Lee, D.K. Dogutan, D.G. Nocera, Hydrogen Generation by Hangman Metalloporphyrins, J. Am. Chem. Soc. 133 (23) (2011) 8775–8777, https://doi.org/10.1021/ja202136y.
[30] D.K. Dogutan, R. McGuire, D.G. Nocera, Electocatalytic Water Oxidation by Cobalt (III) Hangman β-Octafluoro Corroles, J. Am. Chem. Soc. 133 (24) (2011) 9178–9180, https://doi.org/10.1021/ja202138m.
[31] D.K. Dogutan, D.K. Bediako, T.S. Teets, M. Schwalbe, D.G. Nocera, Efficient Synthesis of Hangman Porphyrins, Org. Lett. 12 (5) (2010) 1036–1039, https://doi.org/10.1021/ol902947h.
[32] R. McGuire Jr., D.K. Dogutan, T.S. Teets, J. Suntivich, Y. Shao-Horn, D.G. Nocera, Oxygen Reduction Reactivity of Cobalt(Ii) Hangman Porphyrins, Chem. Sci. 1 (3) (2010) 411.
[33] D.K. Dogutan, S.A. Stoian, R. McGuire, M. Schwalbe, T.S. Teets, D.G. Nocera, Hangman Corroles: Efficient Synthesis and Oxygen Reaction Chemistry, J. Am. Chem. Soc. 133 (1) (2011) 131–140, https://doi.org/10.1021/ja108904s.
[34] C.H. Lee, D. Villágran, T.R. Cook, J.C. Peters, D.G. Nocera, Pacman and Hangman Metal Tetraazamacrocycles, ChemSusChem 6 (8) (2013) 1541–1544, https://doi.org/10.1002/cssc.201300068.
[35] C.G. Margarit, N.G. Asimow, M.I. Gonzalez, D.G. Nocera, Double Hangman Iron Porphyrin and the Effect of Electrostatic Nonbonding Interactions on Carbon Dioxide Reduction, J. Phys. Chem. Lett. 11 (5) (2020) 1890–1895, https://doi.org/10.1021/acs.jpclett.9b03897.
[36] M. Liu, D.K. Dogutan, D.G. Nocera, Synthesis of Hangman Chlorins, J. Org. Chem. 85 (7) (2020) 5065–5072, https://doi.org/10.1021/acs.joc.9b03465.
[37] C.G. Margarit, C. Schnedermann, N.G. Asimow, D.G. Nocera, Carbon Dioxide Reduction by Iron Hangman Porphyrins, Organometallics 38 (6) (2019) 1219–1223, https://doi.org/10.1021/acs.organomet.8b00334.
[38] G. Givaja, M. Volpe, J.W. Leeland, M.A. Edwards, T.K. Young, S.B. Darby, S. D. Reid, A.J. Blake, C. Wilson, J. Wolowska, E.J.L. McInnes, M. Schröder, J.B. Love, Design and Synthesis of Binucleating Macrocyclic Clefts Derived from Schiff-Base Calixpyrroles, Chem. – Eur. J. 13 (13) (2007) 3707–3723, https://doi.org/10.1002/chem.200600989.
[39] E. Askarizadeh, A.M.J. Devoille, D.M. Boghaei, A.M.Z. Slawin, J.B. Love, Ligand Modifications for Tailoring the Binuclear Microenvironments in Schiff-Base Calixpyrrole Pacman Complexes, Inorg. Chem. 48 (15) (2009) 7491–7500, https://doi.org/10.1021/ic900871g.
[40] G. Givaja, M. Volpe, M.A. Edwards, A.J. Blake, C. Wilson, M. Schröder, J.B. Love, Dioxygen Reduction at Dicobalt Complexes of a Schiff Base Calixpyrrole Ligand, Angew. Chem. Int. Ed. 46 (4) (2007) 584–586, https://doi.org/10.1002/anie.200603201.
[41] E. Askarizadeh, S.B. Yaghoob, D.M. Boghaei, A.M.Z. Slawin, J.B. Love, Tailoring Dicobalt Pacman Complexes of Schiff-Base Calixpyrroles towards Dioxygen Reduction Catalysis, Chem. Commun. 46 (5) (2010) 710–712.
[42] M. Volpe, H. Hartnett, J.W. Leeland, K. Wills, M. Ogunshun, B.J. Duncombe, C. Wilson, A.J. Blake, J. McMaster, J.B. Love, Binuclear Cobalt Complexes of Schiff-Base Calixpyrroles and Their Roles in the Catalytic Reduction of Dioxygen, Inorg. Chem. 48 (12) (2009) 5195–5207, https://doi.org/10.1021/ic9001175.
[43] B.J. Love, A Macrocyclic Approach to Transition Metal and Uranyl Pacman Complexes, Chem. Commun. (22) (2009) 3154–3165, https://doi.org/10.1039/B904189C.

[44] J.W. Leeland, A.M.Z. Slawin, J.B. Love, Mononuclear and Mixed-Metal Dimethyltin Pacman Complexes of a Schiff-Base Pyrrole Macrocycle, Organometallics 29 (4) (2010) 714–716, https://doi.org/10.1021/om901081h.
[45] J.A.M. Devoille, B.J. Love, Double-Pillared Cobalt Pacman Complexes: Synthesis, Structures and Oxygen Reduction Catalysis, Dalton Trans. 41 (1) (2012) 65–72, https://doi.org/10.1039/C1DT11424G.
[46] B.E. Cowie, I. Douair, L. Maron, J.B. Love, P.L. Arnold, Selective Oxo Ligand Functionalisation and Substitution Reactivity in an Oxo/Catecholate-Bridged U IV /U IV Pacman Complex, Chem. Sci. 11 (27) (2020) 7144–7157.
[47] J.M. Veauthier, E. Tomat, V.M. Lynch, J.L. Sessler, U. Mirsaidov, J.T. Markert, Calix[4]Pyrrole Schiff Base Macrocycles: Novel Binucleating Ligands for Cu(I) and Cu(II), Inorg. Chem. 44 (19) (2005) 6736–6743, https://doi.org/10.1021/ic050690d.
[48] J.M. Veauthier, W.-S. Cho, V.M. Lynch, J.L. Sessler, Calix[4]Pyrrole Schiff Base Macrocycles. Novel Binucleating Ligands for μ-Oxo Iron Complexes, Inorg. Chem. 43 (4) (2004) 1220–1228, https://doi.org/10.1021/ic0352001.
[49] C.J. Chang, Z.-H. Loh, C. Shi, F.C. Anson, D.G. Nocera, Targeted Proton Delivery in the Catalyzed Reduction of Oxygen to Water by Bimetallic Pacman Porphyrins, J. Am. Chem. Soc. 126 (32) (2004) 10013–10020, https://doi.org/10.1021/ja049115j.
[50] J. Rosenthal, T.D. Luckett, J.M. Hodgkiss, D.G. Nocera, Photocatalytic Oxidation of Hydrocarbons by a Bis-Iron(III)-μ-Oxo Pacman Porphyrin Using O_2 and Visible Light, J. Am. Chem. Soc. 128 (20) (2006) 6546–6547, https://doi.org/10.1021/ja058731s.
[51] J. Rosenthal, B.J. Pistorio, L.L. Chng, D.G. Nocera, Aerobic Catalytic Photooxidation of Olefins by an Electron-Deficient Pacman Bisiron(III) μ-Oxo Porphyrin, J. Org. Chem. 70 (5) (2005) 1885–1888, https://doi.org/10.1021/jo048570v.
[52] J. Rosenthal, D.G. Nocera, Role of Proton-Coupled Electron Transfer in O-O Bond Activation, Acc. Chem. Res. 40 (7) (2007) 543–553, https://doi.org/10.1021/ar7000638.
[53] J.P. Collman, P.S. Wagenknecht, J.E. Hutchison, Molecular Catalysts for Multielectron Redox Reactions of Small Molecules: The "Cofacial Metallodiporphyrin" Approach, Angew. Chem. Int. Ed. Engl. 33 (15–16) (1994) 1537–1554, https://doi.org/10.1002/anie.199415371.
[54] C.K. Chang, H.Y. Liu, I. Abdalmuhdi, Electroreduction of Oxygen by Pillared Cobalt (II) Cofacial Diporphyrin Catalysts, J. Am. Chem. Soc. 106 (9) (1984) 2725–2726, https://doi.org/10.1021/ja00321a055.
[55] J.P. Collman, M. Marrocco, P.E. Denisevich, C. Koval, F.C. Anson, Potent Catalysis of the Electroreduction of Oxygen to Water by Dicobalt Porphyrin Dimers Adsorbed on Graphite Electrodes, J. Electroanal. Chem. Interf. Electrochem. 101 (1) (1979) 117–122, https://doi.org/10.1016/S0022-0728(79)80085-6.
[56] J.P. Collman, P. Denisevich, Y. Konai, M. Marrocco, C. Koval, F.C. Anson, Electrode Catalysis of the Four-Electron Reduction of Oxygen to Water by Dicobalt Face-to-Face Porphyrins, J. Am. Chem. Soc. 102 (19) (1980) 6027–6036, https://doi.org/10.1021/ja00539a009.
[57] R.R. Durand, C.S. Bencosme, J.P. Collman, F.C. Anson, Mechanistic Aspects of the Catalytic Reduction of Dioxygen by Cofacial Metalloporphyrins, J. Am. Chem. Soc. 105 (9) (1983) 2710–2718, https://doi.org/10.1021/ja00347a032.
[58] R. Guilard, M.A. Lopez, A. Tabard, P. Richard, C. Lecomte, S. Brandes, J. E. Hutchison, J.P. Collman, Synthesis and Characterization of Novel Cobalt Aluminum Cofacial Porphyrins. First Crystal and Molecular Structure of a Heterobimetallic Biphenylene Pillared Cofacial Diporphyrin, J. Am. Chem. Soc. 114 (25) (1992) 9877–9889, https://doi.org/10.1021/ja00051a021.
[59] Y. Le Mest, M. L'Her, N.H. Hendricks, K. Kim, J.P. Collman, Electrochemical and Spectroscopic Properties of Dimeric Cofacial Porphyrins with Nonelectroactive Metal Centers. Delocalization Processes in the Porphyrin.Pi.-Cation-Radical Systems, Inorg. Chem. 31 (5) (1992) 835–847, https://doi.org/10.1021/ic00031a028.
[60] R. Guilard, S. Brandes, C. Tardieux, A. Tabard, M. L'Her, C. Miry, P. Gouerec, Y. Knop, J.P. Collman, Synthesis and Characterization of Cofacial Metallodiporphyrins Involving Cobalt and Lewis Acid Metals: New Dinuclear Multielectron Redox Catalysts of Dioxygen Reduction, J. Am. Chem. Soc. 117 (47) (1995) 11721–11729, https://doi.org/10.1021/ja00152a013.
[61] J.P. Collman, J.E. Hutchison, P.S. Wagenknecht, N.S. Lewis, M.A. Lopez, R. Guilard, An Unprecedented, Bridged Dihydrogen Complex of a Cofacial Metallodiporphyrin and Its Relevance to the Bimolecular Reductive Elimination of Hydrogen, J. Am. Chem. Soc. 112 (22) (1990) 8206–8208, https://doi.org/10.1021/ja00178a077.
[62] J.P. Collman, K. Kim, C.R. Leidner, Synthesis, Characterization, and Electrochemistry of Novel Diruthenium Cofacial Porphyrin Dimers, Inorg. Chem. 26 (7) (1987) 1152–1157, https://doi.org/10.1021/ic00254a034.
[63] J.P. Collman, J.E. Hutchison, M.A. Lopez, R. Guilard, A Stable Dinitrogen Complex of a Ruthenium Cofacial Diporphyrin, J. Am. Chem. Soc. 114 (21) (1992) 8066–8073, https://doi.org/10.1021/ja00047a015.
[64] J.B. Love, A.J. Blake, C. Wilson, S.D. Reid, A. Novak, P.B. Hitchcock, The Syntheses and Structures of Group 1 Expanded Dipyrrolides: The Formation of a 12-Rung Amidolithium Circular Ladder, Chem. Commun. 14 (2003) 1682–1683, https://doi.org/10.1039/B303611A.
[65] D.M.M. Freckmann, T. Dubé, C.D. Bérubé, S. Gambarotta, G.P.A. Yap, Cyclic Di- and Mixed-Valent Ytterbium Complexes Supported by Dipyrrolide Ligands, Organometallics 21 (6) (2002) 1240–1246, https://doi.org/10.1021/om010928f.
[66] S. Bellotto, R. Reuter, C. Heinis, H.A. Wegner, Synthesis and Photochemical Properties of Oligo-Ortho-Azobenzenes, J. Org. Chem. 76 (23) (2011) 9826–9834, https://doi.org/10.1021/jo201996w.
[67] P. Bana, Á. Szigetvári, J. Kóti, J. Éles, I. Greiner, Flow-Oriented Synthetic Design in the Continuous Preparation of the Aryl Piperazine Drug Flibanserin, React. Chem. Eng. 4 (4) (2019) 652–657, https://doi.org/10.1039/C8RE00266E.
[68] B. Trofimov, A. Ivanov, E. Skital'tseva, A. Vasil'tsov, I. Ushakov, K. Petrushenko, A. Mikhaleva, A Straightforward Synthesis of 2-(1-Vinyl-1H-Pyrrol-2-Yl)-1H-Benzimidazoles from 1-Vinyl-1H-Pyrrole-2-Carbaldehydes and o-Phenylenediamine, Synthesis 2009 (21) (2009) 3603–3610.
[69] J.L. Sessler, W.-S. Cho, S.P. Dudek, L. Hicks, V.M. Lynch, M.T. Huggins, Synthesis and Study of a Calixpyrrole-Texaphyrin Chimera: A New Oligopyrrolic Chloride Anion Receptor, J. Porphyr. Phthalocyanines 07 (02) (2003) 97–104, https://doi.org/10.1142/S1088424603000136.
[70] A.J. McNeece, K.A. Jesse, J. Xie, A.S. Filatov, J.S. Anderson, Generation and Oxidative Reactivity of a Ni(II) Superoxo Complex via Ligand-Based Redox Non-Innocence, J. Am. Chem. Soc. 142 (24) (2020) 10824–10832, https://doi.org/10.1021/jacs.0c03244.
[71] V. Artero, M. Fontecave, Solar fuels generation and molecular systems: is it homogeneous or heterogeneous catalysis? Chem. Soc. Rev. 42 (2013) 2338–2356, https://doi.org/10.1039/C2CS35334B.
[72] A. Giraudeau, D. Schaming, J. Hao, R. Farha, M. Goldmann, L. Ruhlmann, A simple way for the electropolymerization of porphyrins, J. Electroanal. Chem. 638 (1) (2010) 70–75, https://doi.org/10.1016/j.jelechem.2009.10.018.